# Optical Measurements of High-Density Helicon Plasma by Using a High-Speed Camera and Monochromators*)

Shimpei WASEDA, Hiroaki FUJITSUKA, Shunjiro SHINOHARA, Daisuke KUWAHARA, Marie SAKATA and Hiroshi AKATSUKA[1)]

*Tokyo University of Agriculture and Technology, 2-24-16 Naka-Cho, Koganei, Tokyo 184-8588, Japan*
[1)]*Tokyo Institute of Technology, 2-12-1 Ookayama, Meguro, Tokyo 152-8550, Japan*

(Received 18 November 2013 / Accepted 30 May 2014)

Electric propulsion is an established high-efficiency method in deep space explorers. However, most of the applied methods feature electrodes in direct contact with the plasma, thus its lifetime is limited by the electrodes' erosion. We developed electrodeless electric propulsion systems in order to overcome this problem, and performed optical measurements to estimate the high-density helicon plasma performance of the systems. The electron and neutral particle density profiles were measured by a high-speed camera, and the velocity of the singly-charged Ar ions was determined by a high-resolution monochromator. Additionally, a preliminary experiment of a spectroscopic method using an intensity ratio based on a collisional radiative model with a CCD monochromator was performed. The plasma parameters were in good agreement with the results obtained by an electrostatic probe, and the non-invasive optical measurements presented here can constitute an effective tool for evaluating an electric propulsion system.



Keywords: electric propulsion, helicon plasma, high-speed camera, monochromator, spectroscopy, intensity ratio, collisional radiative model

DOI: 10.1585/pfr.9.3406125

## 1. Introduction

Deep space explorers require a high-efficiency propulsion system. However, for most of them electric propulsion entails electrodes in direct contact with the plasma, and its lifetime is limited by the electrodes' erosion. Hence there has been an increasing interest in electrodeless electric propulsion. Our project of Helicon Electrodeless Advanced Thruster (HEAT) [1] has been developing electrodeless propulsion systems. One of our proposed systems employs a helicon discharge [2] to produce a dense plasma, accelerated by a rotating magnetic field [3].

While the electrostatic probe is a common tool to measure plasma parameters, it disturbs the plasma flow and its signal is sometimes affected by RF noise. In contrast, optical methods, such as spectroscopic methods are noninvasive and insensitive to noise. This study aims to measure high-density helicon plasma parameters by using a high-speed camera (Photron Co. ltd., FASTCAM SA-5: 1.3 Mfps, $1024 \times 1024$ pixels) and 2 monochromators, a high-resolution monochromator (Ritu Oyo Kougaku Co., ltd., Czerny-Turner type MC-150, 2400 lines/mm grating, 0.006 nm resolution) and a CCD monochromator (Ocean Optics Co. ltd., HR2000+, 0.5 nm resolution, 360 - 792 nm range).

The high-speed camera can acquire 2D emission profiles of neutral particles (Ar I) and singly-charged particles (Ar II) by using interference filters [Ar I, center wavelength (CWL) 420 nm for the line of 419.8 nm produced by the transition 5p[1/2] $\rightarrow$ 4s[3/2]°, full width at half maximum (FWHM) 3 nm, Ar II: CWL 488 nm for the line of 487.9 nm from the transition $3p^4(^3P)4p^2D^\circ \rightarrow 3p^44s^2P$, FWHM 1 nm]. The high-resolution monochromator has sufficient resolution to determine the ion velocity, while the CCD monochromator can simultaneously obtain a wide range of emission spectra.

## 2. Theory

If we assume a Maxwellian electron energy distribution with a uniform electron temperature $T_e$ for an ionizing plasma, the collisional radiative (CR) model [4] allows us to describe the intensities of Ar I ($I_{\mathrm{Ar\,I}}$) and Ar II ($I_{\mathrm{Ar\,II}}$) in relation to the electron density $n_e$ and neutral density $n_0$, as shown below.

$$I_{\mathrm{Ar\,I}}(i \rightarrow j) \propto A_{ij} N_{\mathrm{I}i} \propto n_0 S_{\mathrm{I}i}(T_e, n_e),$$
$$I_{\mathrm{Ar\,II}}(i' \rightarrow j') \propto A_{i'j'} N_{\mathrm{II}i'} \propto n_e S_{\mathrm{II}i'}(T_e, n_e). \quad (1)$$

Here, $A_{ij}$ and $A_{i'j'}$ are the transition probabilities of the $i \rightarrow j$ and $i' \rightarrow j'$ transitions for the Ar atom and the Ar ion, respectively; $N_{Ii'}$ and $N_{IIi'}$ are the number densities of the corresponding levels of the Ar atom and the Ar ion, respectively; $S_{\mathrm{I}i}(T_e, n_e)$ and $S_{\mathrm{II}i'}(T_e, n_e)$ are the population rate coefficients of the ionizing plasma to produce $i$th excited state of the Ar atom and $i'$th excited state of Ar

*author's e-mail: sshinoha@cc.tuat.ac.jp*
*) This article is based on the presentation at the 23rd International Toki Conference (ITC23).

ion, respectively. $S_{\mathrm{I}i}(T_\mathrm{e}, n_\mathrm{e})$ and $S_{\mathrm{II}i'}(T_\mathrm{e}, n_\mathrm{e})$ are calculated from the CR model, and are generally dependent on $T_\mathrm{e}$ and $n_\mathrm{e}$. In the present study, $T_\mathrm{e}$ extends above 2 eV and $10^{17} \le n_\mathrm{e}\,[\mathrm{m}^{-3}] \le 10^{19}$, corresponding to the condition for the non-saturated phase of the ionizing plasma, where the population kinetics of the excited states are not saturated in terms of electron collision processes for the Ar plasma [5]. Under this condition, $S_{\mathrm{I}i}(T_\mathrm{e}, n_\mathrm{e})$ and $S_{\mathrm{II}i'}(T_\mathrm{e}, n_\mathrm{e})$ are approximately proportional to $n_\mathrm{e}$, and consequently Eq. (1) can be approximated as follows.

$$I_{\mathrm{Ar\,I}}(i \to j) \propto n_0 S_{\mathrm{I}i}(T_\mathrm{e}, n_\mathrm{e}) \approx n_0 n_\mathrm{e} S'_{\mathrm{I}i}(T_\mathrm{e}),$$
$$I_{\mathrm{Ar\,II}}(i' \to j') \propto n_\mathrm{e} S_{\mathrm{II}i'}(T_\mathrm{e}, n_\mathrm{e}) \approx n_\mathrm{e}^2 S'_{\mathrm{II}i'}(T_\mathrm{e}). \quad (2)$$

Here, $S'_{\mathrm{I}i}(T_\mathrm{e})$ and $S'_{\mathrm{II}i'}(T_\mathrm{e})$ are rate coefficients that depend only on $T_\mathrm{e}$. From Eq. (2), the $n_\mathrm{e}$ and $n_0$ profiles are deduced by acquiring the emission profiles. Because the emissions measured by the high-speed camera and the monochromators are projections, the asymmetric Abel inversion [6] and algebraic reconstruction technique (ART) [7] was performed to reconstruct the local profiles.

The ion flow velocity $v$ can be obtained from a Doppler shift of the ion velocity distribution function (IVDF), as shown in Eq. (3).

$$v = c\Delta\lambda/\lambda_0. \quad (3)$$

Here, $c$ is the speed of light, $\Delta\lambda$ is the wavelength of the ion Doppler shift and $\lambda_0$ is the original wavelength; $n_\mathrm{e}$ and $T_\mathrm{e}$ can be derived by using an intensity ratio based on the CR model.

## 3. Experimental Setup

The experiments were carried out in the Large Mirror Device (LMD) [8], as shown in Fig. 1. This device consists of a quartz tube and a vacuum chamber. The quartz tube has a tapered shape with inner diameter (i.d.) extending from 100 mm to 170 mm and 1,000 mm axial length. The vacuum chamber has 445 mm i.d. and 1,700 mm length. Ar gas enters the quartz tube from the left flange in Fig. 1, and is ionized by a half helical antenna, 185 mm in length, located between $z = -570$ and $-385$ mm, and fed by an RF power supply with an excitation frequency of 7 MHz and a maximum operating RF power $P_\mathrm{rf}$ of 3 kW. In the region of the antenna, the neodymium permanent magnets generate the divergent magnetic field, in addition to the electromagnets surrounding the device. All measurements were performed in a quartz tube region, as shown in Fig. 1. The high-speed camera is located at $z = -90$ mm, and the optical fiber of the CCD monochromator as well as a double probe is positioned at $z = -110$ mm. The high-resolution monochromator views the plasma with an angle of $-45°$ with respect to the flow direction.

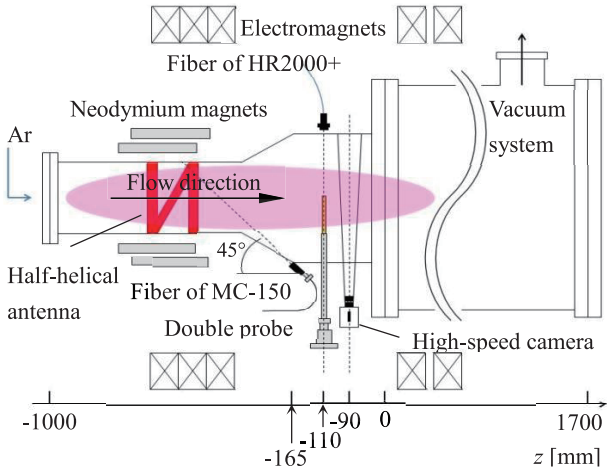


Fig. 1 Schematic view of LMD.

The high-speed camera captures two orthogonal views (inclined at ±45° to the horizontal surface) of the plasma by the use of four 20 mm wide mirrors (two pairs). Each pair, inclined at 0° and 22.5° to the horizontal plane, could lead the plasma emission to the camera. The pairs were positioned at $z = -100$ mm and $-80$ mm, and the local profiles were reconstructed by the slightly different cross sections. Local profiles were extracted in 650 pixels, and the 2D emission profile was reconstructed in $650 \times 650$ pixels by applying the ART method with 10 iterations. The camera's angle of view is 0 - 3°, and we assumed that the decay of intensity by the shift of the CWL is negligible in the emission profiles.

## 4. Experimental Results

Figure 2 shows the radial profiles of $n_\mathrm{e}$ and $T_\mathrm{e}$ obtained by the double probe, and of $n_\mathrm{e}$ acquired by the high-speed camera, using an asymmetric Abel inversion (assuming uniform $T_\mathrm{e}$) with its record speed of 60 fps, $P_\mathrm{rf} = 2$ kW,

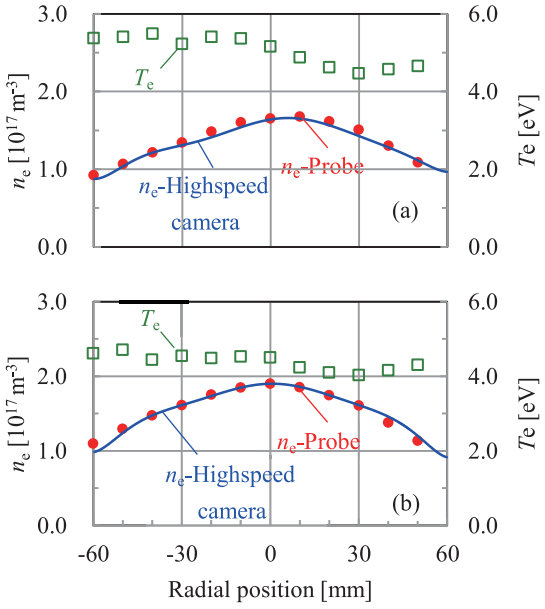


Fig. 2 Radial profile of $n_\mathrm{e}$ and $T_\mathrm{e}$ obtained by the double probe, and of $n_\mathrm{e}$ determined by the high-speed camera with $P_\mathrm{rf} = 2$ kW, and $fr$ = (a) 50 and (b) 70 sccm.

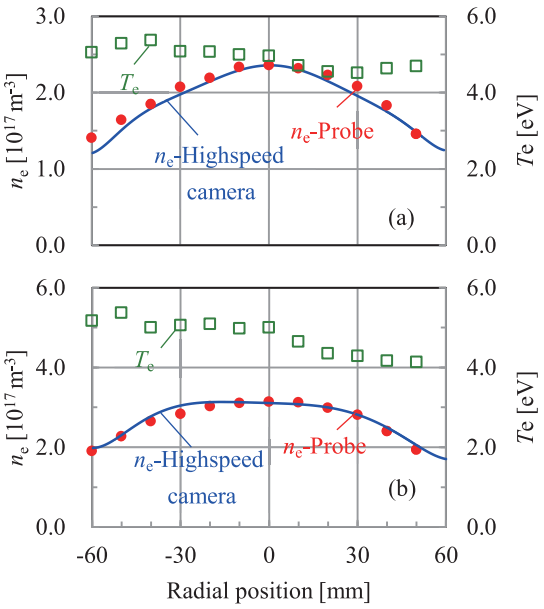


Fig. 3 Radial profiles of $n_e$ and $T_e$ obtained by the double probe and of $n_e$ acquired by the high-speed camera with $P_{rf}$ = 3 kW, and $fr$ = (a) 50 and (b) 70 sccm.

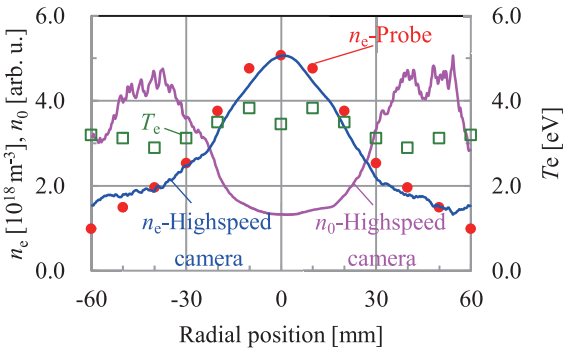


Fig. 4 Radial profiles of $n_e$ and $T_e$ obtained by the double probe, and of $n_e$ and $n_0$ acquired by the high-speed camera, with $P_{rf}$ = 3 kW, $fr$ = 50 sccm and $I_c$ = 300 A.

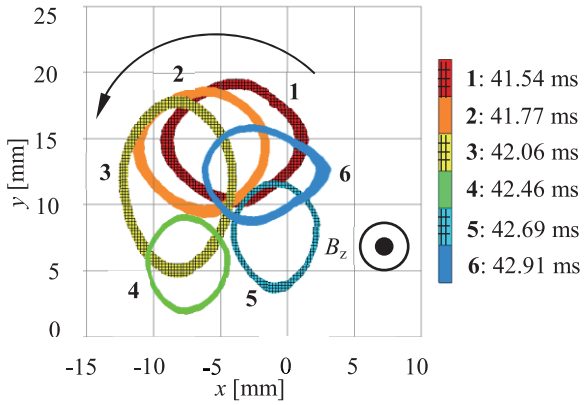


Fig. 5 Time behavior of peak emission intensity (95% level of the maximum intensity) rotating in a high-density plasma cross section.

and gas flow rates $fr$ = 50 and 70 sccm (pressure of 0.67 and 0.84 Pa). The maximum $n_e$ determined by the camera is essentially a relative value, fitted to the maximum $n_e$ obtained by the probe.

There is good agreement between the density profiles obtained with the two methods. Comparing the two results, $n_e$ increases with $fr$ and $T_e$ simultaneously decreases.

Figure 3 shows the radial profiles of $n_e$ and $T_e$ obtained the probe and of $n_e$ acquired by the high-speed camera, recording with 60 fps. Here $P_{rf}$ = 3 kW, $fr$ = 50 and 70 sccm. Again, good agreement is observed between the $n_e$ profiles obtained with the probe and with the camera. From Figs. 2 and 3, $n_e$ with $P_{rf}$ = 3 kW is larger than that with $P_{rf}$ = 2 kW, and $n_e$ in Fig. 3 increases with increasing $fr$, which is also indicated in Fig. 2. However, $T_e$ does not change appreciably with varying $fr$.

The experimental results using electromagnets in addition to permanent magnets are presented in Fig. 4. The experimental parameters are as follows: magnetic coil current $I_c$ = 300 A, $P_{rf}$ = 3 kW, $fr$ = 50 sccm, and the profile obtained with the camera, recorded at 60 fps, was derived by the ART method.

As shown in Fig. 4, the data taken by the probe in the positive radial position are assumed to be the same as those in the negative radial position, because the probe may disturb the plasma near the center, and the maximum $n_0$ is fitted to the maximum $n_e$. While the profile derived by the ART method agrees with that obtained by the probe, the deviation between the profiles is larger in the outer area of the plasma. This is due to the fact that a lack of considerable number of viewing angles causes artifact, especially in the peaked profile, which can be seen by the preliminary simulation. From this figure, $n_0$ displays a hollow profile, while $n_e$ is peaked; neutral particles are ionized in the plasma and thus decrease near the plasma center, which could also be due to higher neutral temperature. Although $n_0$ is expected to have the maximum value in the outer of the plasma, it displays a tendency to decrease near the periphery when the ART method is insufficiently applied.

Figure 5 shows the time behavior of the emission at 95% level of the maximum intensity in a high-density plasma at $P_{rf}$ = 3 kW, $fr$ = 50 sccm, and $I_c$ = 300 A. The camera recorded at 17,500 fps without an interference filter.

Since the intensity of Ar II is much larger than that of Ar I, the obtained profiles can indicate the square of the $n_e$ intensity, as shown in Eq. (1). Although in the present case the ART method is not accurate in the outer region, the peak shift of $n_e$ in the 2D profile is evident. The peak point rotates with a frequency of ~380 Hz in the electron diamagnetic direction within a ~10 mm diameter, the interpretation of this effect requires further detailed measurements.

Figure 6 shows the ion flow velocity along the $z$ axis for varying $fr$ and $P_{rf}$, derived from an ion Doppler shift of the Ar II emission (wavelength 434.8063 nm). The original wavelength of Ar II was measured by an Ar lamp for cali-

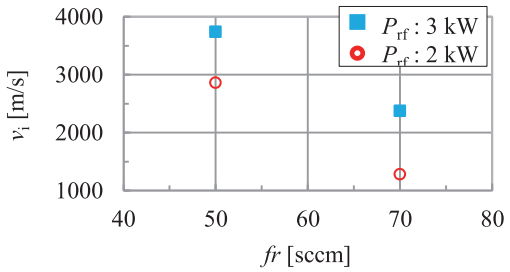


Fig. 6 Ion flow velocity along the $z$ axis for varying $fr$ and $P_{rf}$, using the high-resolution monochromator.

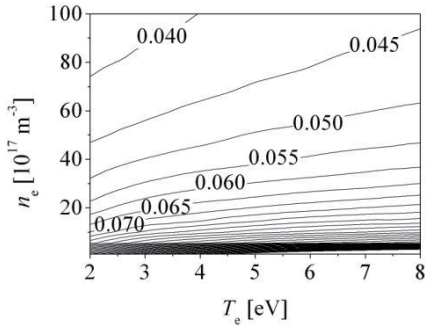


Fig. 7 Contour maps of the intensity ratio of $I$ (675.3 nm)/$I$ (750.4 nm) obtained from a simulation based on the CR model: gas temperature, 500 K; gas pressure, 1 mTorr; plasma radius, 85 mm; $n_e$ is from $10^{17}$ to $10^{19}$ m$^{-3}$, and $T_e$ is from 2 to 8 eV.

Table 1 The radial distribution of the intensity ratio $I$ (675.3 nm)/$I$ (750.4 nm) with $P_{rf}$ = 2 kW and $fr$ = 50 sccm.

| Radial position [mm] | Intensity ratio [arb.u.] |
|---|---|
| 0 | 0.065 |
| 10 | 0.068 |
| 20 | 0.075 |
| 30 | 0.079 |

bration. The ion flow velocity increases with decreasing $fr$ and increasing $P_{rf}$.

Figure 7 shows the calculated contour maps of the intensity ratio of $I$ (Ar I line of 675.3 nm)/$I$ (Ar I line of 750.4 nm) in the ($T_e$, $n_e$) space, based on the CR model. It is obvious that this ratio decreases (increases) with $n_e$ ($T_e$).

Finally, Table 1 shows this ratio measured by the CCD monochromator with $P_{rf}$ = 2 kW and $fr$ = 50 sccm. Here, the line integral intensities of each wavelength were converted to local ones by the Abel inversion technique. Since the line intensity ratio strongly depends on $n_e$, but not on $T_e$, as shown in Fig. 7, we can calculate $n_e$ from the observed intensity ratio in Table 1 in combination with Fig. 7. The resultant $n_e$ was found to be approximately ten times larger than that obtained by the probe measurement (shown in Fig. 2). One of the possible reasons for this discrepancy in $n_e$ may be the electron energy distribution function (EEDF) of the present helicon plasma, which is considered to have a high-energy tail. The Ar CR model in this study is based on the assumption that the EEDF is Maxwellian. Further investigation is necessary for the improvement of the Ar CR model, particularly to include the effect of the EEDF. Additionally, a more precise calibration of the spectral sensitivity of the system is required. However, the observed intensity ratios increase with the radial position showing the decrease of $n_e$ with radius when $T_e$ is constant (Fig. 6). This tendency is qualitatively consistent with the probes' results (Fig. 2).

## 5. Conclusion

Optical measurements were performed to evaluate the performance of high-density helicon plasmas for electrodeless electric propulsion. The measurements demonstrated the potential of a high-speed camera with interference filters to derive $n_e$ and $n_0$ profiles using inversion techniques. The obtained $n_e$ values are in agreement with electrostatic probe results, and in the higher electron density case, the peaked (hollow) profile of $n_e$ ($n_0$) could be clearly determined. The results show the validity of the camera data, which can be advantageous for cases where the probe cannot be inserted and/or strongly disturbs the plasma. From the probe results, $n_e$ increases with increasing $P_{rf}$ and $fr$. The rotation of the density profile near the maximum region has also been observed.

The CCD monochromator results indicate the possibility that the intensity ratio is useful to estimate $n_e$ and $T_e$ in high-density Ar plasmas. This method can be also applied to high-speed cameras, and offers the possibility to instantaneously capture 2D density and temperature profiles. Additionally, the high-resolution monochromator can measure the ion velocity. These precise, noninvasive methods are clearly effective for measuring the plasma performance for their use in electric propulsion.

## Acknowledgments

We appreciate the useful discussions with the Helicon Electrodeless Advanced Thruster (HEAT) project members. This research has been partially supported by Grants-in-Aid for Scientific Research (S: 21226019) from the Japan Society for the Promotion of Science.

[1] S. Shinohara *et al.*, Trans. Fusion Sci. Technol. **63**, 164 (2013).
[2] R.W. Boswell, Phys. Lett. **33A**, 457 (1970).
[3] I.R. Jones, Phys. Plasmas **6**, 1950 (1990).
[4] J. Vlček, J. Phys. D: Appl. Phys. **22**, 623 (1989).
[5] J. Vlček and V. Pelikán, J. Phys. D: Appl. Phys. **19**, 1879 (1986).
[6] Y. Yasutomo *et al.*, IEEE Trans. Plasma Sci. **PS-9**, 18 (1981).
[7] R. Gordon and G.T. Herman, Int. Rev. Cytol. **38**, 111 (1974).
[8] S. Shinohara, S. Takechi and Y. Kawai, Jpn. Appl. Phys. **35**, 4503 (1996).